Research Square

Preprints are preliminary reports that have not undergone peer review.
They should not be considered conclusive, used to inform clinical practice,
or referenced by the media as validated information.

Numerical Modeling of Nitrate and Sulfate Ion Transport through a Cementitious Concrete Matrix: Case of Underground Water Reservoirs in Aggressive Environments

Bienvenu Ebata-Ndion
Higher National Polytechnic Institute, Marien NGOUABI University
Jarlon Brunel Makela
Higher National Polytechnic Institute, Marien NGOUABI University
Roland Dodji Sodjinou
Higher National Polytechnic Institute, Marien NGOUABI University
Narcisse Malanda
nar6malanda@gmail.com
Higher National Polytechnic Institute, Marien NGOUABI University

Research Article

Keywords: concrete, ion transport, diffusion, nitrates, sulfates, inverse identification, numerical modeling, leaching

Posted Date: November 19th, 2026

DOI: https://doi.org/10.21203/rs.3.rs-11508599/v1

License: This work is licensed under a Creative Commons Attribution 4.0 International License.
Read Full License

Additional Declarations: No competing interests reported.

Numerical Modeling of Nitrate and Sulfate Ion Transport through a Cementitious Concrete Matrix: Case of Underground Water Reservoirs in Aggressive Environments

[1,2] Bienvenu Ebata-Ndion, [1,2]Jarlon Brunel Makela, [1,2]Roland Dodji Sodjinou, [1,2] Narcisse Malanda*

[1] Laboratory of Mechanics, Energy and Engineering, Higher National Polytechnic Institute, Marien NGOUABI University, Brazzaville, Republic of the Congo

[2] Higher Institute of Architecture, Building Planning and Public Works, DENIS SASSOU N'GUESSO University, Kintélé, Republic of the Congo

Abstract

This study proposes a numerical model of nitrate (NO_3^-) and sulfate (SO_4^{2-}) ion transport through eight concrete formulations (F1–F8) produced using locally sourced aggregates from Brazzaville and Pointe-Noire, Republic of the Congo, and formulated with CEM II 42.5N Portland cement. Physicomechanical data, including water-accessible porosity ranging from 8.2 to 14.2% and compressive strength ranging from 22.88 to 40.43 MPa at 90 days, together with experimental ion concentrations obtained in a previous study [1], were used as input data for the inverse identification of transport parameters using the L-BFGS-B algorithm.

Nitrate transport, treated as conservative to a first approximation, is described by a diffusive model based on Fick's law, in which the effective diffusion coefficient (Deff) was the only transport parameter identified. The identified values ranged from 2.63×10^{-11} to 8.07×10^{-11} m²/s and exhibited a close relationship with accessible porosity. The model generally reproduced the relative ranking of the formulations; however, discrepancies of approximately 30–38% were observed for the most compact formulations (F1, F3, and F8). These discrepancies may be associated with transient phenomena not explicitly represented in the model, particularly changes in saturation and capillary effects at the beginning of exposure, which may contribute to the differences observed between simulated and experimental concentrations.

For sulfates, a general one-dimensional diffusion–reaction–source model was formulated to simultaneously represent diffusive transport, interactions with the cementitious matrix, and internal contributions potentially associated with leaching. Rather than imposing a priori classification, the model parameters were independently identified for each formulation through constrained inverse optimization. Joint analysis of the identified parameters, the respective contributions of the diffusive, reaction, and source terms, and the experimental response subsequently made it possible to distinguish three operating regimes: a diffusion-dominated regime for F6, a diffusion–reaction regime for F5, and a regime dominated by a source contribution consistent with internal leaching for F1–F4, F7, and F8.

These results show that inverse identification is not only a tool for estimating transport parameters. When combined with an analysis of the mechanistic contributions of the model, it also makes it possible to identify, a posteriori, the different operating regimes of ion transport in the concretes investigated and to highlight the role of microstructure in their behavior under aggressive environmental conditions.

Keywords: concrete; ion transport; diffusion; nitrates; sulfates; inverse identification; numerical modeling; leaching.

1. Introduction

The transfer of dissolved pollutants through the walls of buried concrete reservoirs represents a potential source of contamination of stored water intended for human consumption, thereby constituting a public health concern. In sub-Saharan Africa, and particularly in the Republic of the Congo, underground water-storage infrastructures are commonly used to supply water to local populations in the cities of Brazzaville and Pointe-Noire. The frequent absence of reliable protection systems or adequate waterproofing increases their vulnerability to contamination from external sources. Among the contaminants that may be encountered, nitrate (NO_3^-) and sulfate (SO_4^{2-}) ions, originating notably from agricultural runoff, domestic effluents, and certain sources of organic matter degradation, may migrate through cementitious materials as a result of exchanges between the external environment and the stored water.

Nevertheless, the durability of concrete structures in aggressive environments is fundamentally governed by the transport properties of the cementitious matrix. In water-saturated porous media, ionic migration can be primarily described by diffusion under a concentration gradient, formulated at the macroscopic scale by Fick's second law [2]. However, the assumption of purely conservative transport does not necessarily apply to all ionic species. Sulfate ions may, in particular, interact with cement hydration products and contribute to the formation of secondary phases such as ettringite and gypsum [3] [4], through interactions with aluminate phases and portlandite [5] [6].

This difference in behavior justifies, within the framework of the present study, the use of a diffusion model for nitrates and a more general diffusion–reaction–source model for sulfates. The respective contributions of these mechanisms are determined through inverse identification rather than being prescribed a priori. This different treatment of the two species is based on their different reactivities with respect to the cementitious matrix. In the present study, nitrate ions are considered to be weakly reactive with respect to the main hydrated cement phases; their interactions with the matrix are therefore assumed to be sufficiently limited to justify the assumption of conservative transport as a first approximation [7].

Conversely, sulfate ions exhibit greater reactivity toward the constituents of the cementitious matrix and may participate in reactions capable of modifying their concentration in the pore solution [3–6]. Mechanisms such as the dissolution or progressive transformation of sulfate-containing phases may, in particular, contribute to delayed internal release [8]. In the present model, this contribution is represented effectively by a source term, whose magnitude is determined through inverse identification. This term therefore does not, by itself, constitute evidence for the presence or dissolution of any particular mineral phase, but rather represents, at an overall level, an internal contribution required to reproduce the experimentally observed behavior.

Recent studies conducted in the Republic of the Congo have focused on the physicomechanical characterization of concretes produced using locally sourced aggregates [9] [10], the microstructural characterization of these concretes by scanning electron microscopy coupled with energy-dispersive spectroscopy (EDS) [10], and the experimental characterization of ion transport at the scale of model reservoirs [1]. These studies showed that locally sourced aggregates produce concretes exhibiting, at 90 days, water-accessible porosities ranging from 8.2% to 14.2% and compressive strengths ranging from 22.88 to 40.43 MPa. The experimental tests also revealed differentiated responses of the formulations with respect to sulfate transport. The experimental concentrations measured during these tests [1] constitute the reference data used for the inverse identification of transport parameters and for the evaluation of the numerical model presented in this article.

The objective of this article is to provide a rigorous comparative analysis of nitrate and sulfate ion transport through the eight concrete formulations by combining: (i) a numerical transport model whose mathematical formulation, boundary conditions, and solution scheme are explicitly described and made strictly consistent with the computational code actually used; (ii) inverse identification of the transport parameters using the L-BFGS-B algorithm; (iii) a quantitative analysis of the influence of formulation parameters on transport properties, distinguishing statistically established relationships from qualitative associations; and (iv) a cautious assessment of the implications of these mechanisms for the durability of concretes intended for drinking-water storage in tropical environments

2. Materials and Methods

2.1. Diffusion Experimental Setup

The experimental data used in this study were obtained from the experimental setup described in detail in [1]. Diffusion tests were conducted in eight rectangular polymer tanks measuring 0.30 m × 0.50 m. Each tank contained a concrete reservoir intended for drinking-water storage, with internal dimensions of 0.25 m × 0.35 m and a uniform wall thickness of 0.05 m. The annular space between the reservoir and the external tank was filled with fine sand saturated with the contaminant solution, over a width of approximately 7.5 cm in the longitudinal direction and 5 cm in the transverse direction. The reservoirs were manufactured using the

different formulations investigated and subsequently water-cured for 28 days in accordance with NF EN 12390-2 [11]. The external aggressive solution was prepared from nitrate and sulfate stock solutions at concentrations of 2.5 g/L and 4.334 g/L, respectively, and diluted in the diffusion tanks (25 L) to obtain initial concentrations of $C_0(NO_3^-)$ = 30 mg/L and $C_0(SO_4^{2-})$ = 52 mg/L, expressed as NO_3^- and SO_4^{2-} ions, respectively (HACH NitraVer® 5, ISO 7890, λ = 520 nm, and SulfaVer® 4, NF T90-040, λ = 650 nm methods, which directly determine the ionic species rather than the corresponding salts). The external concentrations were maintained constant by renewing the solution every two weeks throughout the twelve-week exposure period, at a controlled temperature of 23 ± 2 °C. The concentrations reported in this study are those measured in the drinking water stored inside the reservoirs, i.e., the concentrations that had effectively diffused through the concrete wall.

2.2. Description of the Concrete Formulations Investigated

Eight concrete formulations were investigated using the Dreux–Gorisse method. They differed in aggregate type and size (rounded versus crushed aggregates), geographical origin (Brazzaville: F1–F4; Pointe-Noire: F5–F8), proportion of crushed sand (30–50%), and water-to-cement (W/C) and coarse-to-fine aggregate (G/S) ratios. The complete characterization of the aggregates and the physicomechanical properties was carried out in previous studies to which the present study refers [9] [10] [1]. Table 1 summarizes these data.

Table 1. *Composition and physicomechanical properties of formulations F1–F8 [9] [10] [1].*

Formulation	W/C	G/S	Aggregate composition	Porosity (%) 28d	Porosity (%) 90d	Compressive strength (MPa) 28d	Compressive strength (MPa) 90d	Real density (g/cm³) 28d	Real density (g/cm³) 90d
F1	0.49	2.45	Crushed gravel (10/14 + 5/15) Kombé + Congo River sand	10.5	8.4	33.75	37.13	2.41	2.43
F2	0.49	1.80	F1 + 50% crushed Inkissi sandstone sand (Kombé)	13.4	10.2	26.65	29.32	2.37	2.38
F3	0.49	2.43	Crushed gravel + Mfilou river sand	9.8	8.2	36.75	40.43	2.44	2.45
F4	0.49	1.70	Mfilou sand + 40% crushed sand	12.5	9.4	27.25	29.98	2.39	2.41
F5	0.47	3.06	Rounded gravel (3/8) Mboubissi + local sand	14.6	10.8	22.80	25.08	2.26	2.30
F6	0.47	1.70	F5 + 50% improved crushed sand	15.6	14.2	18.30	22.88	2.25	2.28
F7	0.49	2.36	Crushed Louvouvou granite + local sand	13.6	9.2	27.30	32.12	2.37	2.38
F8	0.49	1.89	F7 + 50% improved crushed sand	11.0	9.0	29.70	32.67	2.35	2.37

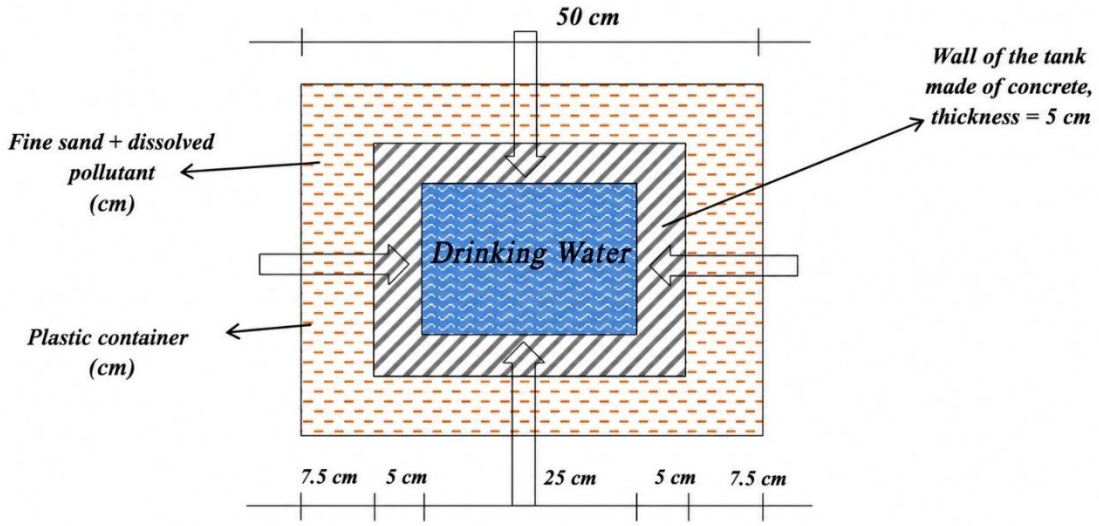


***Figure 1**: Simplified diagram of the experimental diffusion setup [12].*

2.3. Numerical Transport Model

2.3.1. General Equation and Assumptions

The transport of an ionic species with concentration C(x,t) through the concrete wall is described, in a reactive porous medium, by the conservation equation coupled with Fick's law [13] [14] [15] :

$$\varphi(x)\cdot\partial C/\partial t = \partial/\partial x[\varphi(x)\cdot Deff(x)\cdot\partial C/\partial x] - \varphi(x)\cdot k\cdot C(x,t) + \varphi(x)\cdot S(x,t),\ \forall x \in (0,L),\ t > 0 \quad (1)$$

where $\varphi(x) \in (0,1]$ denotes the accessible porosity of the concrete, $Deff(x) > 0$ is the effective diffusion coefficient (m^2/s), $k \geq 0$ is the first-order reaction-rate constant (s^{-1}) representing the consumption or chemical binding of ions, and $S(x,t) \geq 0$ representing an internal release of ions compatible with the progressive dissolution of hydrated phases.

Although concrete is a porous, heterogeneous, and multiphase material, it is homogenized at the macroscopic scale for each formulation. Accordingly, its transport properties are considered constant across the wall thickness for a given formulation and curing age. In contrast, the experimental domain represented in the model remains heterogeneous and multiphase, since it successively comprises contaminated sand, the concrete wall, the reservoir water, the second concrete wall, and the opposing contaminated sand. The porosity $\varphi(x)$ and effective diffusion coefficient $Deff(x)$ are therefore defined by zones and may exhibit discontinuities at the interfaces between materials.

Within each zone where φ and $Deff$ are constant, Equation (1) reduces to:

$$\varphi \cdot \partial C/\partial t = \varphi \cdot Deff \cdot \partial^2 C/\partial x^2 - \varphi \cdot k \cdot C + \varphi \cdot S \quad (2)$$

The free-solution diffusivities are set to $D_0 = 1.99 \times 10^{-9}$ m²/s for nitrates and $D_0 = 1.11 \times 10^{-9}$ m²/s for sulfates [16] [17]. These values serve as reference diffusivities for identifying the effective diffusion coefficients in concrete.

2.3.2. Boundary Conditions and Coupling with the Reservoir Water

Since the domain is symmetric with respect to the median plane of the reservoir, the two concrete walls are considered to be subjected to the same exposure conditions and are represented symmetrically in the model.

At the soil–concrete interface, a Dirichlet condition imposes a constant source concentration:

$$C(0,t) = C_0,\ \forall t>0 \quad (3)$$

At the concrete–reservoir interface, exchange with the stored water is represented by a Robin boundary condition:

$$-Deff \cdot \partial C/\partial x|_{x=l} = h \cdot [C(L,t) - Cint(t)],\ t>0 \quad (4)$$

where h (m/s) denotes the effective exchange coefficient at the concrete–water interface, C(L,t) is the concentration of the ionic species at the internal face of the concrete, and Cint(t) is the corresponding concentration in the reservoir water.

The initial condition is defined as:

$$C(x,0) = 0,\ \forall x \in [0, L] \quad (5)$$

This condition represents the initial state of the concrete before exposure to the contaminated solution.

2.3.3. Numerical Discretization and Stability Condition

The spatial domain [0,L] is discretized into N = 100 uniform control volumes. Concentrations are evaluated at the centers of the control volumes, with a width $\Delta x = L/N = 5 \times 10^{-3}$ m. This discretization makes it possible to explicitly represent the two concrete walls as well as the sand zones located on either side of the reservoir.

The diffusion coefficient at the interface between two adjacent control volumes is calculated using the harmonic mean in order to ensure physical continuity of the diffusive flux at the interface between two media with different diffusivities, particularly between sand and concrete:

$$D_{i+1/2} = 2 \cdot Di \cdot D_{i+1} / (Di + D_{i+1}) \quad (6)$$

By integrating Equation (2) over the control volume centered at x_i between t^n and $t^{n+1} = t^n + \Delta t$ and applying an explicit Euler scheme, the equation obtained for the interior node i ($2 \le i \le N-1$) is:

$$C_i^{n+1} = C_i^n + \Delta t/\varphi_i \cdot \{[D_{i+1/2} \cdot (C_{i+1}^n - C_i^n) - D_{i-1/2} \cdot (C_i^n - C_{i-1}^n)]/\Delta x^2 - k \cdot C_i^n + S\} \quad (7)$$

The scheme is explicit, does not require the solution of a linear system, and is subject to the corresponding Courant–Friedrichs–Lewy (CFL) stability condition:

$$\Delta t \le C_{CFL} \cdot \varphi_min \cdot \Delta x^2 / (2 \cdot Dmax) \quad (8)$$

For $\Delta x = 5 \times 10^{-3}$ m and Deff on the order of 10^{-10}–10^{-11} m²/s, this condition imposes an internal integration time step on the order of several tens of seconds to a few minutes, which is considerably shorter than the weekly interval between experimental measurements. The internal time step is therefore systematically adjusted to satisfy Equation (8), while concentrations are extracted at the weekly time points corresponding to the measurement campaigns, over a total simulation period of T = 12 weeks.

2.3.4. Inverse Parameter Identification

The parameter vector to be identified depends on the ionic species considered. For nitrates, only the effective diffusion coefficient Deff is identified, while the parameters k and S are set to zero in accordance with the assumption of conservative behavior.

For sulfates, the parameter vector $\theta = \{Deff, k, S, h\}$ is identified simultaneously by minimizing the least-squares objective function:

$$J(\theta) = \Sigma_t [\ Cexp(t) - Cnum(\theta, t)\ ]^2 \quad (9)$$

where Cexp(t) is the experimental value at time t and Cnum(θ,t) is the corresponding numerical concentration at the outlet node. The L-BFGS-B algorithm is used subject to the following physical constraints: $Deff \in [10^{-13}, 10^{-9}]$ m²/s ; $k \in [0, 10^{-6}]$ s⁻¹ ; $S \in [0, 10^{-5}]$ mg·L⁻¹·s⁻¹ ; $h \in [10^{-8}, 10^{-4}]$ m/s.

3. Results

3.1. Nitrate Ion Transport (NO_3^-)

3.1.1 Temporal Evolution of Numerically Simulated Concentrations in the Different Concrete Formulations

To quantify nitrate ion transport in the different concrete formulations, numerical modeling based on Fick's second law was performed using a Python code developed for this purpose. The simulated concentrations over twelve weeks are presented in Table 2.

Table 2. *Simulated nitrate ion concentrations obtained by numerical modeling*

Time (week)	*Simulated nitrate ion concentrations from numerical modeling* (mg/L)							
	F1	**F2**	**F3**	**F4**	**F5**	**F6**	**F7**	**F8**
1st	0,00000	0,00000	0,00000	0,00000	0,00000	0,00000	0,00000	0,00000
2nd	0,00741	0,04283	0,00634	0,03090	0,05537	0,06065	0,02070	0,01062
3rd	0,04877	0,17412	0,04373	0,13559	0,21105	0,24144	0,10299	0,06292
4th	0,10877	0,32472	0,09934	0,26024	0,38436	0,44581	0,20722	0,13475
5th	0,17519	0,47653	0,16158	0,38793	0,55707	0,64938	0,31634	0,21236
6th	0,24346	0,62561	0,22592	0,51452	0,72555	0,84695	0,42553	0,29114
7th	0,31185	0,77096	0,29060	0,63881	0,88894	1,03732	0,53331	0,36947
8th	0,37967	0,91231	0,35488	0,76041	1,04709	1,22027	0,63920	0,44674
9th	0,44663	1,04963	0,41846	0,87917	1,19999	1,39591	0,74304	0,52272
10th	0,51264	1,18296	0,48122	0,99508	1,34778	1,50442	0,84476	0,59736
11th	0,57765	1,31238	0,54310	1,10817	1,43057	1,69605	0,94439	0,67066
12th	0,64167	1,43799	0,60410	1,21849	1,51853	1,78106	1,04194	0,74264

Table 1 highlights a progressive increase in the simulated concentrations for all formulations, characteristic of a non-steady-state diffusion regime controlled by the concentration gradient between the aggressive environment and the concrete.

At 12 weeks, the concentrations range from 0.604 mg/L for F3 to 1.781 mg/L for F6.

Formulations F6, F5, and F2 exhibit the highest concentrations, indicating greater susceptibility to nitrate diffusion. Conversely, F3 and F1 show the lowest values, confirming the influence of a denser microstructure in limiting ion transport.

To analyze the temporal dynamics of this diffusion and compare the evolution of the different formulations, the numerical results presented in Table 1 are plotted in Figure 2.

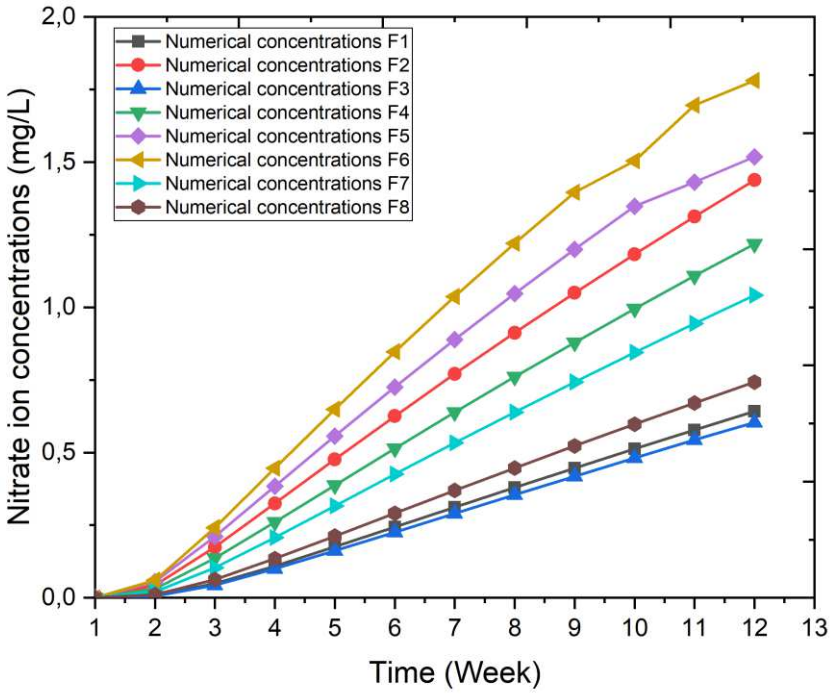


Figure 2: *Temporal evolution of numerically simulated nitrate ion concentrations in the different concrete formulations*

Figure 2 confirms the hierarchy observed in the table. The curves corresponding to F6, F5, and F2 exhibit the steepest slopes, indicating faster nitrate ion diffusion. Conversely, F3 and F1 maintain the lowest transport rates, reflecting greater resistance to ion transport due to lower porosity and reduced capillary connectivity.

These results are consistent with the microstructural correlations established previously and show that nitrate mobility mainly depends on the compactness of the cementitious matrix. They therefore provide the basis for identifying the effective diffusion coefficient, which is analyzed in the following section.

3.1.2 Evolution of Diffusion Coefficients at 28 and 90 Days

The effective diffusion coefficients (Deff) identified by inverse optimization are of the order of 10^{-11} m²/s, consistent with values reported for saturated concretes based on Portland cement [18] [19] [20]. Table 3 summarizes the coefficients determined at 28 and 90 days, together with the associated microstructural and mechanical parameters [1].

Tableau 3*. Effective diffusion coefficients of NO_3^- ions and associated microstructural and mechanical parameters (porosity and Rc according to [1])*

Formulation	Deff 28j ($\times10^{-11}$ m²/s)	Deff 90j ($\times10^{-11}$ m²/s)	ΔD ($\times10^{-11}$)	Cmax 12 sem. (mg/L)	Porosité 90j (%)	Rc 90j (MPa)
F1	2,96	2,89	0,07	1,01	8,4	37,13
F2	5,69	5,53	0,16	1,44	10,2	29,32
F3	2,68	2,63	0,05	0,97	8,2	40,43
F4	4,82	4,69	0,13	1,25	9,4	29,98
F5	6,66	6,47	0,19	1,63	10,8	25,08
F6	8,29	8,07	0,22	1,88	14,2	22,88
F7	4,02	3,91	0,11	1,15	9,2	32,12
F8	3,53	3,44	0,09	1,07	9,0	32,67

The most porous formulations (F5: 10.8%; F6: 14.2% at 90 days) exhibit the highest diffusion coefficients (6.47–8.07 × 10^{-11} m²/s), whereas F1 and F3 combine low porosities (8.4% and 8.2%) with low diffusion coefficients (2.89 and 2.63 × 10^{-11} m²/s, respectively).A systematic decrease in Deff between 28 and 90 days is observed, averaging approximately 2.5%, reflecting the progressive densification of the microstructure resulting from continued hydration reactions [21].

Figure 3 highlights the temporal evolution of the effective diffusion coefficients (Deff) between 28 and 90 days and provides an assessment, for each formulation, of the effect of material maturation on nitrate ion transport properties.

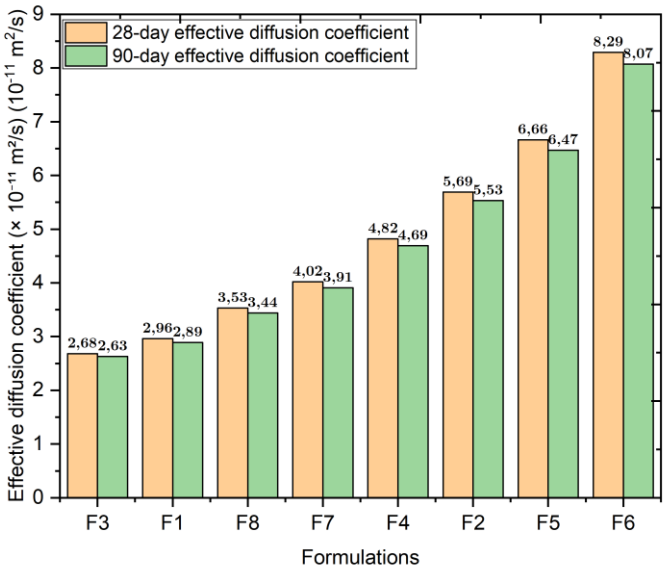


***Figure 3**: Evolution of the effective diffusion coefficients Deff between 28 and 90 days.*

Figure 3 confirms the limited evolution of **Deff** with concrete age. Despite a systematic decrease between 28 and 90 days, the differences remain limited for all formulations, indicating a moderate evolution of the diffusive properties over the period investigated.

3.1.3 Correlations between Porosity, Compressive Strength, and Diffusivity

The experimental results reveal a strong correlation between accessible porosity and the effective nitrate diffusion coefficient at 90 days. Across the eight formulations, porosity ranges from 8.2 to 14.2%, whereas Deff ranges from 2.63 × 10^{-11} to 8.07 × 10^{-11} m²/s. The relationship between Deff and accessible porosity (φ) is described by a second-degree polynomial regression with a high coefficient of determination (R^2 = 0.986), with the least porous formulations generally exhibiting the lowest diffusivities.

Figure 4 jointly presents the correlations between Deff, accessible porosity, and compressive strength at 90 days.

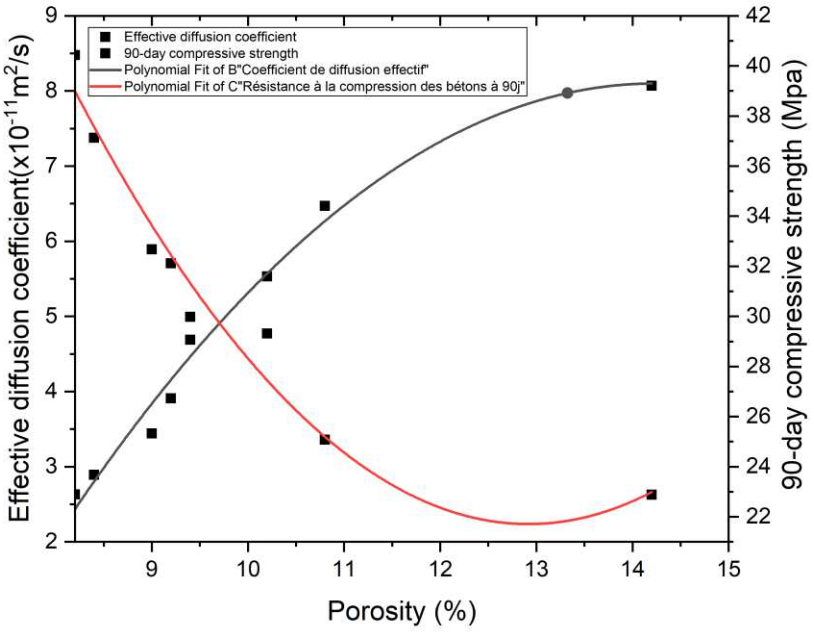


***Figure 4**: Correlations between the effective nitrate diffusion coefficient, accessible porosity, and compressive strength at 90 days.*

A strong negative correlation is also observed between Deff and compressive strength, with $R^2 = 0.973$ and adjusted $R^2 = 0.963$. Thus, increasing porosity is accompanied by a decrease in mechanical strength and an increase in diffusivity.

A comparison of the extreme formulations illustrates this trend. F3, with a porosity of 8.2%, exhibits the highest compressive strength (40.43 MPa) and the lowest diffusivity (2.63×10^{-11} m²/s), whereas F6, with 14.2% porosity, exhibits the lowest compressive strength (22.88 MPa) and the highest diffusivity (8.07×10^{-11} m²/s). The difference in diffusivity therefore reaches a factor of approximately 3.1, while the W/C ratios are very similar, suggesting that the differences in transport are also related to the microstructural state of the material. This evolution likely reflects a common state of compactness underlying both mechanical properties and transport, without implying that compressive strength directly controls diffusion.

The strong empirical correlation between Deff and porosity suggests that the overall state of the pore structure is a major determinant of diffusive transport in the formulations investigated. This relationship is consistent with the studies reported in [22] [23] [24], which respectively emphasize the importance of the organization and connectivity of the pore network, as well as percolation phenomena, in the transport properties of cementitious materials.Within the range investigated, accessible porosity therefore constitutes a relevant global indicator of diffusivity, although it does not allow the respective contributions of pore connectivity, tortuosity, and constrictivity to be distinguished.

Scanning electron microscopy (SEM) observations performed on the same formulations [10] provide complementary insight. At the microstructural scale, the formulations containing rounded aggregates, F5 and F6, exhibit large aggregate clusters separated by inter-aggregate voids and apparently less homogeneous bonding between the paste and aggregates, whereas F1 and F3 exhibit a more continuous and compact organization. These observations of the interfacial transition zone (ITZ) [10] [25] [26] are compatible with a possible contribution of interface organization to pore-network connectivity and, consequently, to transport pathways. However, they do not allow the respective contributions of the ITZ, connectivity, and tortuosity to be established directly in the absence of independent measurements of these parameters.

The differences observed between formulations containing crushed aggregates and those containing rounded aggregates should also be interpreted with caution. The formulations with angular crushed aggregates, F1, F3, and F7, exhibit lower Deff values ($2.63–3.91 \times 10^{-11}$ m²/s) than the formulations with rounded aggregates, F5 and F6 ($6.47–8.07 \times 10^{-11}$ m²/s).

However, these formulations simultaneously differ in geographical origin, particle-size distribution, sand type, as well as G/S and W/C ratios. Since the experimental design was not factorial, the specific effect of aggregate type cannot therefore be statistically isolated from the other formulation factors.

Similarly, the G/S ratio does not exhibit a systematic relationship with the effective diffusion coefficient. Although formulations F1 and F3 combine high G/S ratios with low diffusivities, this trend cannot be generalized: F5, which has the highest G/S ratio in the series (3.06), conversely exhibits a high diffusivity (6.47×10^{-11} m²/s). The G/S ratio therefore cannot be considered independently as a reliable predictor of ion transport. Thus, within the range investigated, nitrate diffusivity is strongly associated with the overall compactness of the material, for which accessible porosity constitutes the macroscopic descriptor showing the strongest empirical relationship with Deff.

Compressive strength evolves in the opposite direction, while SEM observations suggest a complementary role of interface organization and pore-network connectivity. However, these results should be interpreted as relationships observed within the investigated series rather than as evidence of a direct causal relationship. A more comprehensive description of diffusivity would require independent measurements of pore-network connectivity, tortuosity, and constrictivity.

3.1.4 Validation of the Diffusion Model

Validation of the diffusion model is based on a comparison between the experimental concentrations [1] and the concentrations obtained from numerical simulations for the eight formulations. Table 4 presents the measured and calculated concentrations at 12 weeks, together with the corresponding relative deviations, thereby providing a quantitative assessment of the model's ability to reproduce the experimental results.

Tableau 4. *Differences between experimental and numerical NO_3^- ion concentrations at 12 weeks*

Formulation	Experimental concentrations (mg/L)	Numerical concentrations (mg/L)	Relative deviation (%)
F1	1,01	0,642	36,5
F2	1,44	1,438	0,1
F3	0,97	0,604	37,7
F4	1,25	1,218	2,5
F5	1,63	1,519	6,8
F6	1,88	1,781	5,3
F7	1,15	1,042	9,4
F8	1,07	0,743	30,6

The results in Table 3 show that the model reproduces the experimental concentrations with good accuracy for F2, F4, F5, F6, and F7, with relative deviations below 10% at 12 weeks.

In contrast, a greater underestimation is observed for F1, F3, and F8, with deviations of 36.5%, 37.7%, and 30.6%, respectively. These deviations are associated with the formulations exhibiting the most compact matrices and indicate that the simple diffusion model does not reproduce all the observed behaviors with the same level of accuracy.

This difference in model performance suggests that the simplifying assumptions adopted, particularly the homogeneity of the medium and the absence of an explicit representation of initial capillary effects, may become limiting for the densest matrices.

Thus, the results do not support the conclusion that the model faithfully reproduces the experimental observations for all formulations. Rather, they demonstrate that the model is capable of representing the general transport trend, with accuracy varying according to the formulation.

Comparison of the temporal evolutions provides further insight into the model performance. Figure 5 presents the experimental and numerical concentrations obtained for the eight formulations over the entire 12-week period.

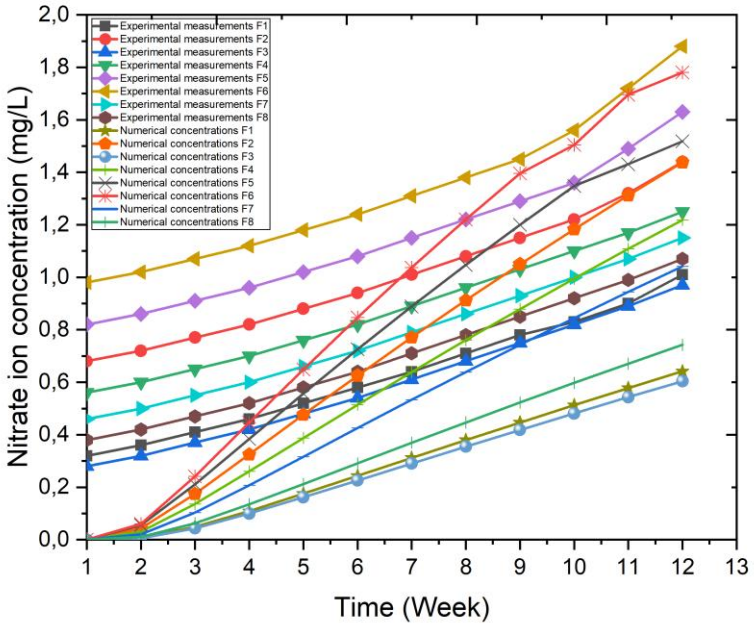


***Figure 5**: Comparison of experimental [1] and numerical NO_3^- ion concentrations for the eight formulations over 12 weeks*

Comparison of the curves shows progressive convergence between the numerical and experimental results, particularly from approximately the 6th–8th weeks onward. This evolution indicates that, despite the deviations observed for certain formulations at 12 weeks, the diffusive description adequately captures the general transport trend at advanced exposure ages. It therefore confirms that diffusion constitutes the dominant mechanism governing nitrate transport under the experimental conditions investigated, while also highlighting the limitations of the model for the most compact matrices.

3.2. Sulfate Ion Transport (SO_4^{2-})

3.2.1 Parameters Identified for the Diffusion–Reaction–Source Model

The identified values of the effective diffusion coefficient (*Deff*), the reaction coefficient (*k*), the source term (*S*) and the exchange coefficient (*h*) are presented in Table 5.

Table 5. *Identified model parameters for formulations F1 to F8*

Formulation	Deff 28d (m^2/s)	Deff 90d (m^2/s)	k (s^{-1})	S ($mg \cdot L^{-1} \cdot s^{-1}$)	h (m/s)
F1	1.6×10^{-10}	1.45×10^{-10}	0	3.8×10^{-7}	1.0×10^{-7}
F2	1.8×10^{-10}	1.62×10^{-10}	0	4.2×10^{-7}	1.1×10^{-7}
F3	1.2×10^{-10}	1.08×10^{-10}	0	2.5×10^{-7}	9.0×10^{-8}
F4	1.5×10^{-10}	1.35×10^{-10}	0	2.0×10^{-7}	1.0×10^{-7}
F5	1.4×10^{-10}	1.26×10^{-10}	1.1×10^{-6}	0	8.0×10^{-8}
F6	2.1×10^{-10}	1.89×10^{-10}	0	0	1.2×10^{-7}
F7	2.0×10^{-10}	1.80×10^{-10}	0	5.2×10^{-7}	1.1×10^{-7}
F8	1.3×10^{-10}	1.17×10^{-10}	0	3.0×10^{-7}	9.5×10^{-8}

The effective diffusion coefficients at 90 days range from 1.08×10^{-10} m²/s for F3 to 1.89×10^{-10} m²/s for F6. Formulations F3 and F8 exhibit the lowest diffusivities, whereas F6 and F7 show the highest values. Within the series investigated, these values reflect the influence of the pore-structure state on sulfate-ion mobility, consistent with the relationships established for cementitious materials [3][19].

The reaction coefficient is zero for most formulations and is non-zero only for F5 ($k = 1.1 \times 10^{-6}$ s^{-1}). The source term is positive for F1–F4, F7, and F8, with values ranging from 2.0×10^{-7} to 5.2×10^{-7} mg·L^{-1}·s^{-1}, whereas it is zero for F5 and F6. The exchange coefficient h remains between 8.0×10^{-8} and 1.2×10^{-7} m/s, i.e., within the same order of magnitude across all formulations.

These results show that the differences between formulations cannot be described by the effective diffusion coefficient alone. The differentiated presence of the k and S terms indicates that, depending on the formulation, the transport kinetics also require the representation of a reactive contribution or an effective internal input. The h coefficient, which is relatively invariant, appears to be a less discriminating parameter among the formulations [2][27].

3.2.2 Origin of the Transport Regimes: Contribution of Modeling to Mechanistic Interpretation

The three sulfate transport regimes previously identified experimentally [1] can be interpreted from the D_{eff}, k, and S parameters identified by the model. F6, characterized by k = 0 and S = 0, corresponds to transport primarily controlled by diffusion. Its high diffusivity at 90 days (1.89×10^{-10} m²/s) is consistent with its high porosity (14.2%) and low mechanical strength (22.88 MPa), in agreement with the role of pore-network structure and connectivity in ionic transport through cementitious materials [22].

F5 is characterized by the presence of a non-zero reactive term ($k = 1.1 \times 10^{-6}$ s^{-1}) in the absence of a source term. Within the model framework, this contribution reflects a progressive consumption of sulfates during transport, consistent with the interactions between sulfates and hydrated phases described in [28][4][6].

Conversely, F1–F4, F7, and F8 exhibit k = 0 and require a positive source term to reproduce the experimental concentrations. This contribution represents an effective internal input consistent with reactive-transport approaches incorporating the dissolution, release, and transformation phenomena of the cementitious matrix reported in [29][30]. Reactive-transport models applied to cementitious materials indeed show that diffusion processes can be coupled with chemical reactions capable of modifying concentrations in solution.

The term S, however, must be interpreted as an effective model parameter and not as a direct measurement of a particular chemical mechanism. Its presence indicates that diffusion alone is insufficient to reproduce the measured concentrations. It is consistent with a release associated with the evolution of the cementitious matrix, although its precise origin cannot be established from transport data alone. The numerical analysis thus complements the experimental identification of the transport regimes by distinguishing, within the model framework, the contributions associated with diffusive transport, reaction, and effective internal input

.3.2.3 Coupling between microstructure and chemical reactivity

Comparison of the formulations shows that a decrease in diffusivity is not systematically accompanied by a decrease in internal chemical activity. F5 and F8 particularly illustrate this dissociation: F5 exhibits a non-zero reactive term and a zero source term, whereas F8 exhibits k = 0 and a positive source term. Thus, low diffusivity alone is not, in itself, an indicator of chemical stability.

This dissociation is also apparent for F2 and F7, which exhibit the highest values of the source term *S*, even though their diffusion coefficients remain lower than that of F6. The observed concentration differences therefore cannot be attributed solely to sulfate mobility, but also involve, within the model framework, an effective internal contribution.

Conversely, F6 combines the highest diffusivity with k = 0 and S = 0. Its behavior is thus mainly governed by the accessibility of the pore network, with no identified contribution from the reactive and source terms.

The exchange coefficient *h*, which varies relatively little between formulations, does not constitute a major discriminating factor. The differences in behavior are thus mainly associated, within the identification framework, with the parameters *Deff*, *k* and *S*. These results highlight that microstructure and reactivity constitute two complementary dimensions of formulation behavior. A more compact structure can limit diffusive transport without necessarily eliminating the internal contributions needed to describe the experimental concentrations. This dissociation leads to a joint examination of the microstructural parameters and those derived from model identification.

3.2.4 Microstructural threshold and organization of transport mechanisms

The preceding results show that the organization of the transport mechanisms cannot be described using a single microstructural indicator. It results from the combination of porosity, mechanical strength, and the identified model parameters.

Figure 6 presents the distribution of the formulations within the microstructural space defined by the porosity–compressive strength pair (ϕ, *Rc*).

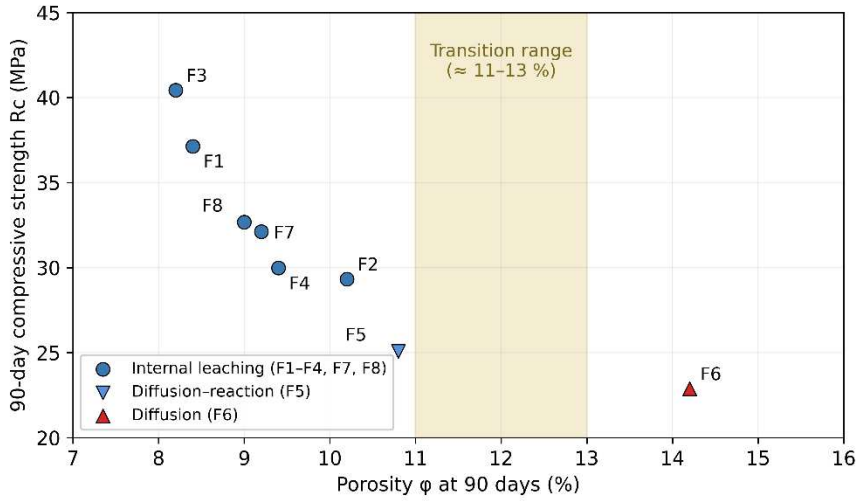


Figure 6: *Distribution of formulations in the microstructural space (ϕ, Rc)*

The most porous formulations generally exhibit the highest diffusion coefficients, whereas the more compact formulations show lower ionic mobility. However, formulations with relatively similar microstructural characteristics can develop different chemical behaviors. Description by ϕ and *Rc* alone is therefore not sufficient to account for all the observed kinetics.

Figure 7 complements this representation by locating the formulations in the (ϕ, $k + S$) space, in order to relate the microstructural state to the reactive and source contributions identified by the model.

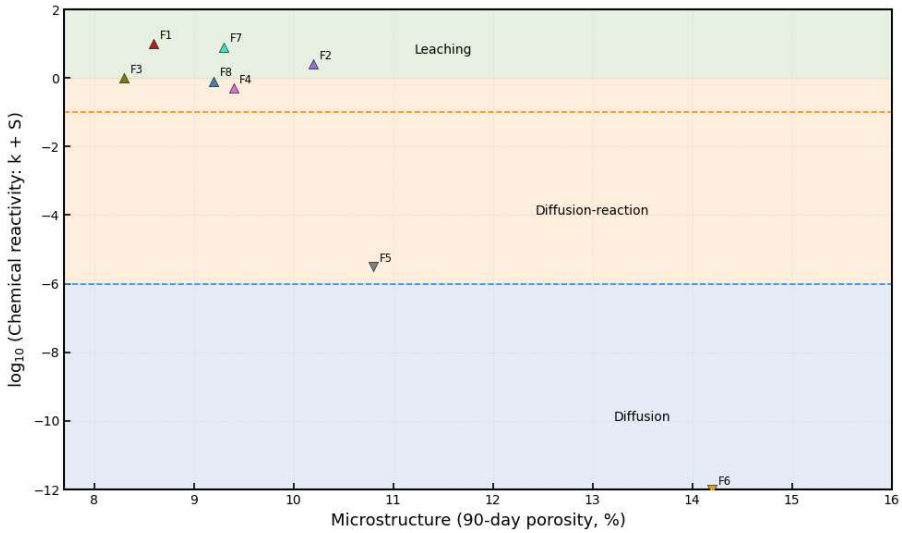


Figure 7: *Organization of the formulations according to microstructure and reactivity parameters (ϕ, k + S)*

Within the series of concrete formulations studied, the transition between behaviors appears approximately within a porosity range of 11 to 13%. Beyond this range, F6 (ϕ = 14.2%) exhibits behavior dominated by diffusion. Below it, F5 (ϕ = 10.8%) is associated with a reactive contribution, while F1–F4, F7 and F8 show a positive source contribution.

This organization should, however, be interpreted as a trend observed within the domain studied and not as a universal physical threshold. The limited number of formulations and the non-factorial nature of the experimental design do not allow for the establishment of a critical value independent of the formulation.

The microstructural characteristics and identified parameters for the three transport regimes are summarized in Table 6.

Table 6. *Summary of transport mechanisms according to microstructural parameters (ϕ, Rc) and model parameters (Deff, k, S).*

Regime	Formulations	ϕ (%)	Rc (MPa)	Deff (m^2/s)	k (s^{-1})	S ($mg \cdot L^{-1} \cdot s^{-1}$)
Diffusion	F6	14,2	22,9	$1,89\times10^{-10}$	0	0
Diffusion–reaction	F5	10,8	25,1	$1,26\times10^{-10}$	$1,1\times10^{-6}$	0
Diffusion–source	F1–F4, F7–F8	8,2–10,2	29,3–40,4	$1,08–1,80\times10^{-10}$	0	$2,0–5,2\times10^{-7}$

Taken together, these results show that the transport mechanisms are organized according to a combination of microstructural and physico-chemical factors. Within this framework, *Deff* primarily reflects the diffusive component of transport, while *k* and *S* respectively represent the reactive and source contributions needed to describe the experimental kinetics.

The microstructural threshold should thus be considered a multidimensional transition zone rather than a single value of porosity or mechanical strength. The joint identification of *Deff*, *k* and *S* provides a coherent framework for relating the microstructural state of the formulations to the different sulfate transport behaviors observed experimentally

3.2.5 Validation of the diffusion–reaction–source model

Validation of the model is assessed by direct comparison between the experimental [1] and numerical concentrations for the three transport regimes identified previously. The results show a good capacity of the model to quantitatively reproduce the observed kinetics, with deviations that remain limited over the full twelve weeks of exposure.

For the diffusive regime represented by F6 (k = 0; S = 0), the simulated concentrations correctly follow the experimental evolution. The relative deviations, on the order of 10–12% during the first weeks, progressively decrease to approximately 6% at the twelfth week. The two curves evolve in parallel without cumulative divergence (Figure 8), indicating that the model correctly reproduces the kinetics when transport is primarily controlled by diffusion.

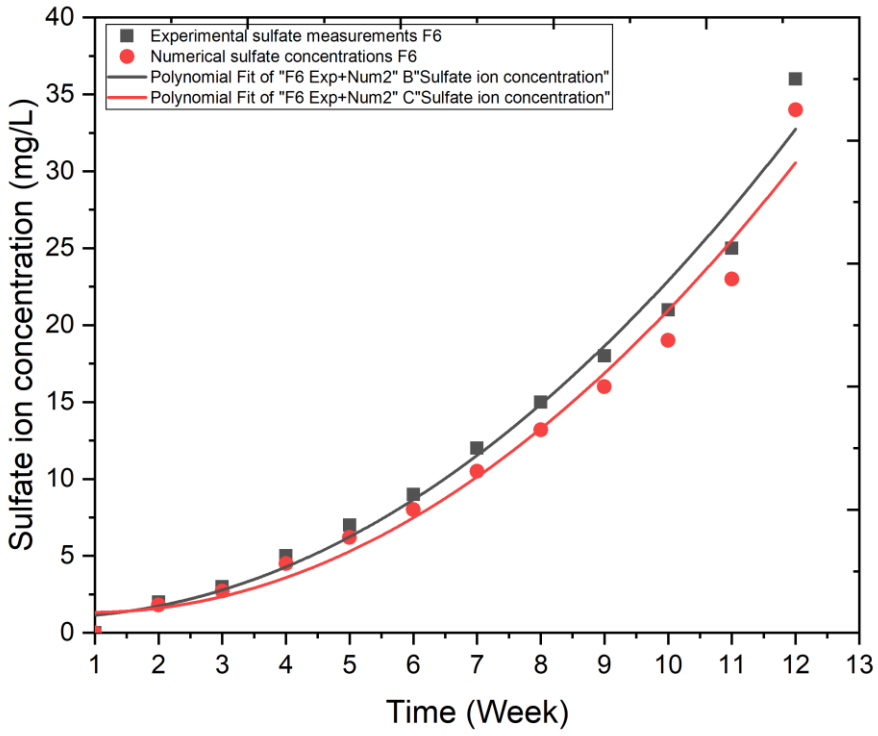


Figure 8: *Comparison of experimental and numerical SO_4^{2-} ion concentrations for formulation F6.*

For the diffusion–reaction regime represented by F5, the agreement between the experimental and numerical results is particularly high (Figure 9). Absolute deviations remain at 0.01 mg/L over the entire period, while relative deviations decrease from 10% to approximately 3%. The model thus accurately reproduces the small progressive increase in concentration observed experimentally, quantitatively confirming its capacity to represent the kinetics combining diffusive transport with a reactive term.

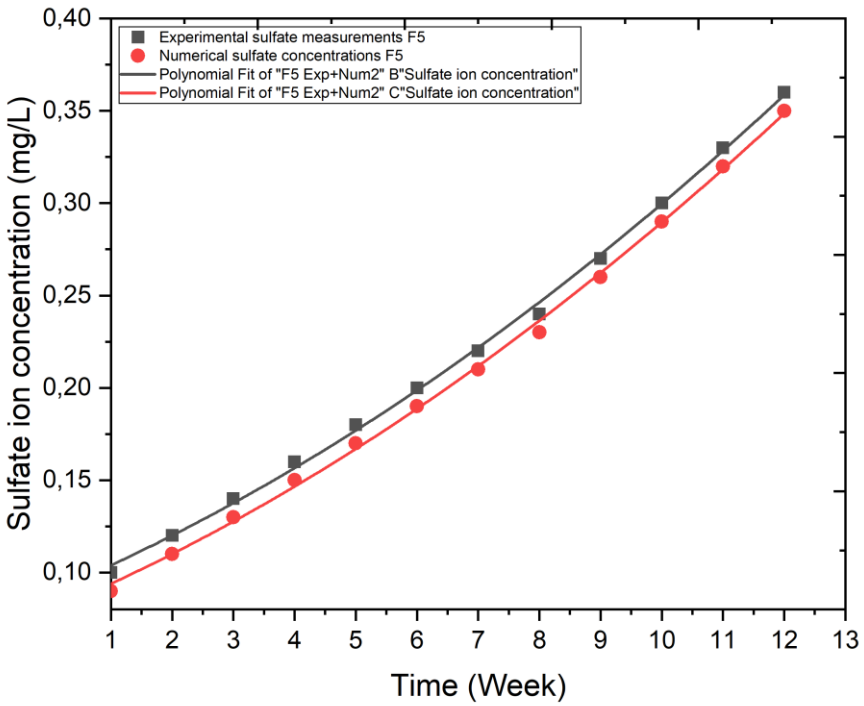


Figure 9: *Comparison of experimental and numerical SO_4^{2-} ion concentrations for formulation F5.*

For formulations F1–F4, F7 and F8, characterized by a positive source term, the simulations correctly reproduce the concentration levels and their temporal evolution (Figure 10). A slight underestimation is observed in the early stages of exposure, but the numerical trajectories remain close to the measurements and notably reproduce the ranking of concentrations between formulations. Agreement is particularly evident for formulations F2 and F7, which exhibit the highest concentrations. These results show that the introduction of the source term makes it possible to reproduce kinetics experimentally characterized by an effective internal input.

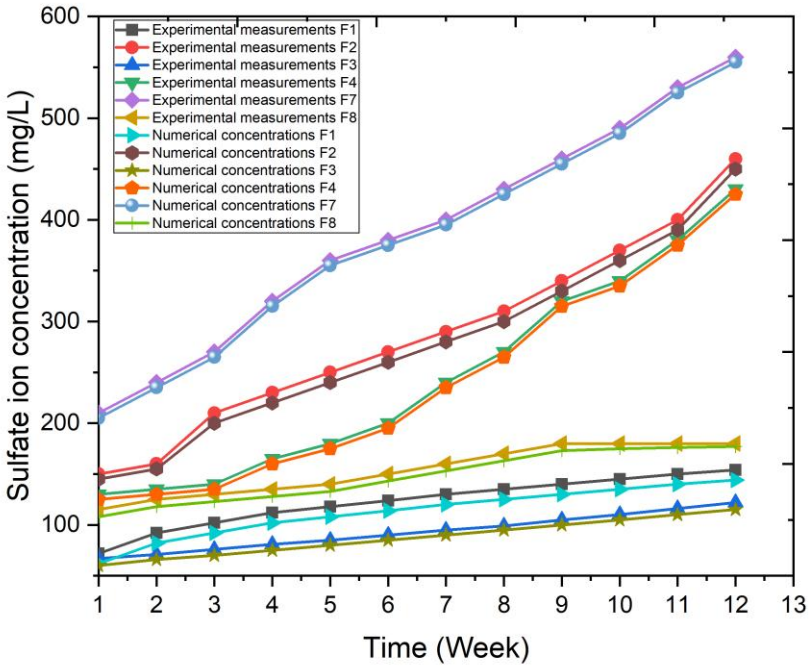


Figure 10: *Comparison of experimental and numerical SO_4^{2-} ion concentrations for formulations F1–F4, F7 and F8.*

The overall comparison of the eight formulations (Figure 11) confirms the model's capacity to reproduce the different concentration levels and kinetics observed experimentally over the twelve weeks of exposure. The simulations show no systematic drift and correctly reproduce the three identified behaviors: dominant diffusion, diffusion–reaction, and diffusion–source. The residual deviations, mainly observed in the early stages of exposure, remain consistent with the simplifying assumptions of the model, in particular the use of constant parameters. Taken together, these results confirm that the diffusion–reaction–source model provides a consistent quantitative representation of the experimental observations for the eight formulations studied.

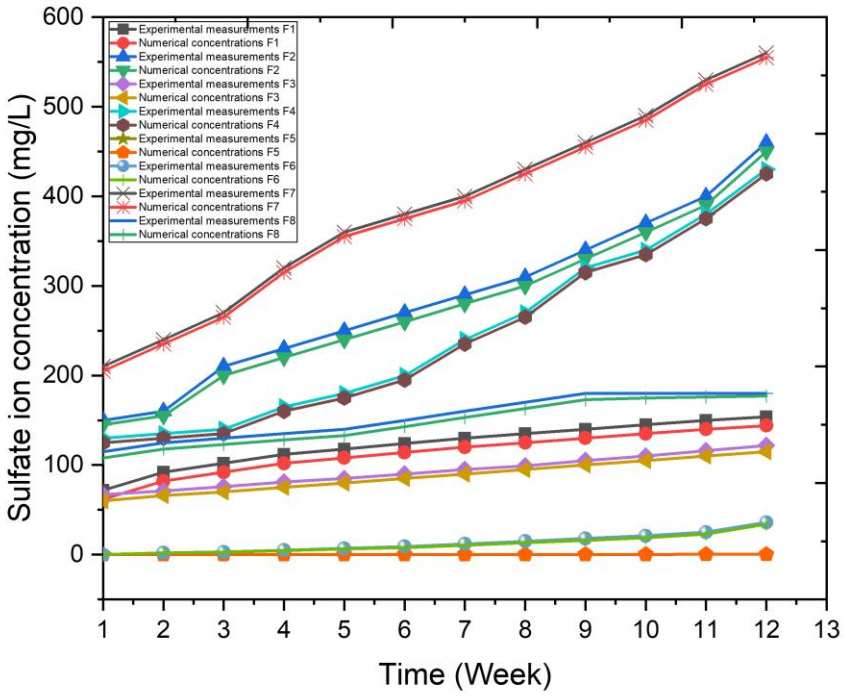


Figure 11: *Overall comparison of experimental and numerical SO_4^{2-} ion concentrations for the eight formulations over twelve weeks.*

3.2.6 Statistical indicators and evaluation of model performance

Model performance was evaluated using three complementary indicators: the root mean square error (RMSE), the coefficient of determination (R^2), and the mean bias. The values obtained for the eight formulations are summarized in Table 7.

Table 7. Statistical indicators of the simulations for the eight formulations.

Formulation	Transport regime	RMSE (mg/L)	R^2	Bias (mg/L)
F1	Internal leaching	3.2	0.996	−1.2
F2	Internal leaching	4.5	0.995	−1.5
F3	Internal leaching	2.8	0.997	−0.8
F4	Internal leaching	3.0	0.996	−1.0
F5	Diffusion–reaction	0.02	0.999	−0.01
F6	Pure diffusion	1.5	0.998	−0.5
F7	Internal leaching	7.5	0.991	−3.0
F8	Internal leaching	3.5	0.995	−1.1

The R^2 values, ranging between 0.991 and 0.999, indicate strong agreement between the simulated and experimental concentrations for all formulations. The best fit is obtained for F5 (R^2 = 0.999; RMSE = 0.02 mg/L), while F7 shows the highest root mean square error (RMSE = 7.5 mg/L) and the lowest R^2 (0.991). These deviations nonetheless remain small relative to the measured concentrations, which reach up to 560 mg/L.

The bias is negative for all formulations, with values ranging between −0.01 and −3.0 mg/L, reflecting a slight general tendency of the model to underestimate the experimental concentrations. This tendency is particularly pronounced for F7, but remains modest relative to the concentration levels reached.

Taken together, these indicators confirm the good quality of the reproduction of the experimental data by the diffusion–reaction–source model. They complement the experimental–numerical comparison presented previously by providing a quantitative assessment

of error, agreement, and bias. The statistical performance obtained thus shows that the model satisfactorily describes the sulfate transport kinetics for the eight formulations studied, including when the contribution of a source term is required.

3.2.7 Comparison of nitrate and sulfate behavior in cementitious materials

The results reveal a fundamental difference between nitrate and sulfate transport. Nitrates exhibit essentially diffusive behavior and can be described using the effective diffusion coefficient (*Deff*) alone, whereas sulfates exhibit reactive behavior requiring, in addition to *Deff*, the introduction of terms representing reaction (*k*) and effective internal input (*S*). This difference reflects the distinct nature of the interactions between the two ionic species and the cementitious matrix.

The main differences between the two species in terms of transport, interaction with the matrix, and representation by the model are summarized in Table 8.

Table 8. *Summary comparison of nitrate and sulfate behavior in cementitious materials.*

Aspect	Nitrates (NO_3^-)	Sulfates (SO_4^{2-})
Nature of transport	Essentially diffusive	Reactive
Interaction with the matrix	Weak	Strong
Dominant mechanism	Diffusion	Diffusion–reaction–source
Model parameters	Deff	Deff, k, S, h
Regimes observed	Diffusive	Diffusion, diffusion–reaction, diffusion–source
Secondary products	Not identified	Ettringite, gypsum
Sensitivity to porosity	Direct control of transport	Control coupled with reactivity
Predictability	High	More dependent on internal processes

For nitrates, the absence of a significant reactive contribution thus makes it possible to interpret *Deff* mainly as a function of the accessibility and connectivity of the pore network. Conversely, for sulfates, ionic mobility alone is not sufficient to describe the measured concentrations: the identification of *k* and *S* shows that interactions with the matrix and internal inputs must be taken into account. Reactions between sulfates and cementitious phases can in particular lead to the formation of secondary ettringite and gypsum [31], while the dissolution of internal phases can contribute an additional input of sulfate species [32][5].

Figure 12 summarizes this distinction by contrasting the essentially diffusive transport of nitrates with the diffusion–reaction–source transport of sulfates. It thus shows that the higher complexity of the model used for sulfates does not result from a difference in the magnitude of diffusivity, but from the need to represent additional physico-chemical contributions.

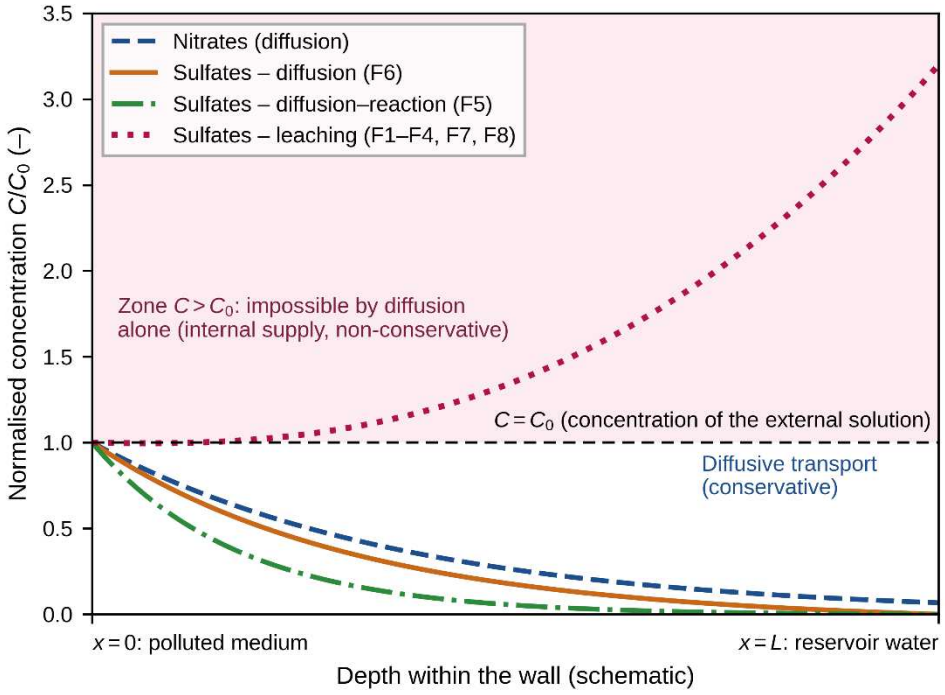


Figure 12: *Comparative conceptual diagram of nitrate and sulfate transport in cementitious materials.*

The effective sulfate diffusion coefficients obtained in this study, ranging between 1.08×10^{-10} and 2.10×10^{-10} m²/s, remain of the same order of magnitude as those reported for cementitious materials exposed to sulfates [32][33]. The observed differences may be related to the specific characteristics of the formulations and the exposure conditions. Thus, comparison of the two species shows that *Deff* is a relevant indicator of ionic mobility, but that its interpretation must be supplemented by reactive parameters when the transported species interacts with the cementitious matrix.

3.2.8 Implications for the design of underground reservoirs

This section examines the implications of the results obtained for the design of underground water reservoirs exposed to humid tropical and chemically aggressive environments. The objective is to assess to what extent the requirements of EN 206 [34] account for the actual durability of the formulations studied, and to identify complementary parameters likely to improve design. The analysis thus compares the normative criteria with the experimental performance and the transport and reactivity mechanisms highlighted by the modeling.

3.2.8.1 Regulatory framework

The EN 206 standard [34] defines concrete durability requirements according to environmental exposure classes. In the case of the underground water reservoirs studied, the conditions mainly correspond to classes XC2/XC3 (humid environments) and XA1 to XA3 (chemically aggressive environments), classified according to soluble sulfate content and aggressive ion levels in water, in accordance with Annex D of EN 206. The standard prescribes overall criteria (W/C, strength class, composition), presumed to guarantee a microstructure dense enough to limit ionic transfer. These requirements nonetheless remain indirect and do not make it possible to explicitly describe the transport and reaction mechanisms within the cementitious matrix [35][36].

3.2.8.2 Assessment of formulation compliance with EN 206

The formulations studied generally meet the requirements of the EN 206 standard, with W/C ratios ranging between 0.47 and 0.49 and strength classes mostly greater than or equal to C30/37. This finding confirms that the water/cement ratio, although closely related to capillary porosity, does not on its own constitute a sufficient indicator of durability [37].

However, the experimental and modeling results reveal strongly differentiated ionic transport behaviors that this compliance alone does not allow one to anticipate.

To compare the normative criteria with the actual behavior of the materials, Table 9 presents a cross-summary of performance.

Table 9. *Summary of normative performance and actual behavior of the formulations*

Formulation	Target class	W/C	Measured Rc	EN 206 compliance	Porosity	NO_3^- diffusivity ($\times 10^{-11}$ m²/s)	SO_4^{2-} behavior	Actual durability
F1	XC3/XA2	0.49	≥ C30/37	Compliant	Low	2.89	Reactive	High
F2	XC3/XA2	0.49	< C30/37	Compliant	Moderate	5.53	Reactive	Good
F3	XC3/XA3	0.49	≥ C30/37	Compliant	Low	2.63	Reactive (strong fixation)	Excellent
F4	XC3/XA2	0.49	< C30/37	Compliant	Moderate	4.69	Reactive	Good
F5	XC3/XA2	0.47	< C30/37	Partial	High	6.47	Diffusive (weak reaction)	Critical long-term
F6	XC3/XA2	0.47	< C30/37	Partial	High	8.07	Diffusive (pure)	Moderate to low
F7	XC3/XA2	0.49	< C30/37	Compliant	Moderate	3.91	Reactive	Good
F8	XC3/XA2	0.49	< C30/37	Compliant	Low	3.44	Reactive (strong)	High

The results show that compliance with EN 206 requirements alone does not guarantee satisfactory durability in a sulfate environment. Thus, formulations with similar normative characteristics can develop very different transport behaviors. Formulation F3 combines low diffusivity, low porosity and high mechanical strength, reflecting a good ability to limit the penetration of aggressive species. Conversely, formulations F5 and F6 exhibit higher diffusion coefficients despite comparable water/cement ratios, illustrating the limitations of an approach based solely on formulation parameters.

Analysis of the behavior toward sulfates also reveals a marked distinction between formulations. Concretes F1 to F4, as well as F7 and F8, exhibit reactive behavior dominated by leaching and internal chemical transformation phenomena, related to the progressive dissolution of cement hydrates and the formation of secondary phases such as ettringite and gypsum [33][31]. Formulation F5 stands out for a regime in which diffusive transport is accompanied by chemical interactions with cement hydrates, while F6 exhibits behavior essentially controlled by diffusion owing to its more open microstructure.

These observations confirm that concrete durability results from a close coupling between the pore structure, which governs the transport mechanisms, and the chemical reactivity of the matrix, which controls the fixation or release of aggressive species. They highlight the limitations of exclusively prescriptive approaches, which do not explicitly take into account the internal physico-chemical phenomena responsible for material evolution in aggressive environments. In agreement with the analyses of Alexander et al. [38] and Baroghel-Bouny [39], these results show that durability assessment should be supplemented by performance indicators directly linked to the transport properties and chemical reactivity of cementitious materials.

3.2.8.3 Toward an integrated performance-based approach to durability

The results obtained show that, beyond a certain level of compactness — characterized by low porosity, high mechanical strength and increased chemical stability — the ionic transport mechanisms become significantly more limited. This observation highlights the limitations of a normative approach based solely on the water/cement ratio and strength class, since formulations compliant with EN 206 requirements can exhibit substantially different transport and durability behaviors.

From this perspective, the integration of physically interpretable parameters, such as the effective diffusion coefficient (Deff), the reaction coefficient (k) and the source term (S), appears essential to simultaneously characterize the transport and chemical reactivity phenomena. This approach, in line with the principles of the performance-based methods proposed by the fib Model Code [40], naturally leads to defining design criteria based on the mechanisms actually governing the durability of cementitious materials.

3.2.8.4 Recommendations for the design of underground reservoirs in humid and aggressive environments

The experimental and numerical results obtained show that the design of concretes intended for humid and chemically aggressive environments, particularly underground water reservoirs, would benefit from a performance-based approach explicitly integrating the material's microstructure, ionic transport properties and internal chemical interactions, in addition to the requirements of the EN 206 standard [39][38].

For underground water reservoirs located in humid and chemically aggressive environments, particularly of the XA2 to XA3 type, the results obtained thus lead to favoring formulations combining a compact microstructure, low diffusivity and good chemical stability. Within the domain studied, it appears particularly relevant to favor crushed aggregates, which promote the development of a more compact microstructure and lower diffusion coefficients than rounded aggregates, and to aim for an accessible porosity below 10%. Crossing a porosity zone close to 11–12% is indeed accompanied by a significant increase in transport phenomena and degradation under sulfate exposure.

Formulations combining low diffusivity, reduced porosity and good chemical stability, such as F1, F3 and F8 within the domain studied, thus appear more favorable to reservoir durability. Conversely, the more porous formulations, in particular F5 and F6, require additional design or in-service monitoring measures. These recommendations should, however, be considered within the experimental domain of this study and do not constitute universal thresholds independent of the formulation and exposure conditions.

These recommendations directly reflect the experimental and numerical findings obtained and illustrate the value of a design approach based on performance criteria adapted to humid tropical environments rich in sulfates.

Ultimately, this study shows that the durability of concretes exposed to aggressive environments cannot be guaranteed by compliance with EN 206 requirements alone. It results from the coupling between microstructure, ionic transport properties and the chemical reactivity of the cementitious matrix. Its assessment thus benefits from a performance-based approach integrating physically interpretable indicators, combined with the modeling of transport mechanisms, in accordance with the guidelines of the fib Model Code [40]. Such an approach provides a more reliable framework for the design and prediction of the long-term durability of underground water reservoirs located in the humid tropical environments of the Republic of Congo.

4. Discussion

The results obtained first show that the transport of nitrate and sulfate ions cannot be described by the same transfer mechanism across the eight formulations studied. For nitrates, the effective diffusion coefficients obtained at 90 days range from 2.63×10^{-11} to 8.07×10^{-11} m²/s and show a strong correlation with accessible porosity ($R^2 = 0.986$). This ranking places formulations F3, F1 and F8 among the least diffusive, while F6 and F5 exhibit the highest diffusivities. This trend is also consistent with the decrease in diffusivity as mechanical strength increases, with matrix compactness thus constituting an important macroscopic factor in ionic transport. The available data indicate, however, that porosity and strength alone are not sufficient to explain all the differences observed between formulations.

This relationship between porosity and diffusivity is consistent with models describing ionic transport in cementitious materials as depending not only on accessible pore volume, but also on the structure of the transport network. Percolation-based approaches show in particular that diffusivity depends on the fraction of effectively connected pores and the geometry of the pore network, rather than on total porosity alone [23][41][24].

In the formulations studied, the strong correlation obtained between porosity and Deff therefore constitutes a macroscopic indicator consistent with this interpretation. It does not, however, make it possible to experimentally dissociate the respective contributions of connectivity, tortuosity and constrictivity, which were not independently measured in the present work.

The ranking of the formulations is also consistent with the influence of aggregate nature and particle size distribution on the structure of the matrix and the interfacial transition zone. The SEM-EDS observations carried out on the same formulations [10] show that the characteristics of the interfacial transition zone may contribute to the differences in behavior observed between crushed and rounded aggregates [18][26]. This interpretation must nonetheless remain cautious: the SEM-EDS observations used here mainly provide qualitative information on local morphology and composition and do not, on their own, allow quantification of the tortuosity, connectivity or constrictivity of the pore network. The link between aggregate nature, microstructure and transport should therefore be regarded as a convergent interpretation of the results rather than as a directly demonstrated causal relationship.

The Deff values obtained for nitrates otherwise remain within the orders of magnitude reported for ordinary Portland-cement-based concretes. In particular, they fall within the ranges reported for concretes of comparable strength and within the order of magnitude of 10^{-11} m²/s generally reported for ordinary cementitious matrices [41][37][20]. This agreement supports the physical plausibility of the identified coefficients, despite the specific characteristics of the local aggregates and experimental conditions. Differences between studies must nevertheless be interpreted with caution, since diffusivity values depend in particular on the W/C ratio, the age and degree of saturation of the concrete, the experimental method used, the nature of the ion studied, and the method used to identify Deff [42][25]. Comparison with the literature thus constitutes more of an order-of-magnitude check than a direct comparison of values obtained under strictly identical conditions.

For sulfates, the behavior appears qualitatively different. The identified coefficients, ranging between 1.08×10^{-10} and 2.10×10^{-10} m²/s, are higher than those obtained for nitrates and must be interpreted as apparent coefficients, integrating, within the framework of the model adopted, the combined effects of transport, reaction and internal release. This difference therefore does not mean that sulfates intrinsically diffuse faster than nitrates in free solution. Rather, it reflects the reactive nature of the sulfate–cementitious matrix system, which distinguishes these two species in terms of their behavior in concrete [28].

The main value of inverse identification appears precisely at this level. An increase in the concentration of sulfates in the receiving solution, particularly when it exceeds the imposed external concentration, could a priori be attributed either to an increase in diffusive transfer or to a progressive release of species originating from the matrix. These two mechanisms can produce temporal evolutions of relatively similar shape. The simultaneous determination of the parameters Deff, k, S and h, without imposing a transport regime on each formulation beforehand, makes it possible to examine these different contributions within the framework of the model adopted. Inverse identification thus constitutes more than a numerical fitting procedure: it provides a means of differentiating effective behaviors that cannot be sufficiently robustly distinguished by observation of the experimental curves alone.

This analysis leads to the distinction of three regimes within the domain studied: a diffusion-dominated regime for F6, a diffusion–reaction regime for F5, and a diffusion–source regime for F1–F4, F7 and F8. Formulation F7 constitutes the most pronounced case, with a sulfate concentration reaching 560 mg/L, well above the imposed initial concentration. The introduction of the source term S thus makes it possible to reproduce behavior that could not be represented by a classical diffusive model alone. Release and dissolution phenomena involving species present in cementitious materials have already been reported in various contexts [29][43][30]. In the present work, however, the term S must be interpreted as an effective source term: its identification does not on its own demonstrate that it specifically originates from the dissolution of portlandite, AFm phases, or another cementitious phase. A mechanistic attribution would require additional analyses of the solution and solid phases, in particular by chemical speciation, XRD, and targeted SEM-EDS analyses.

The quality of the fits obtained for sulfates ($R^2 = 0.991–0.999$) confirms that the model accurately reproduces the kinetics measured over the twelve weeks used for identification. However, these coefficients of determination should be interpreted as goodness-of-fit indicators rather than as independent predictive validation. The same data were indeed used to calibrate and then evaluate the model's reproduction. In the absence of an independent dataset, cross-validation, or a complementary experimental campaign, the model's ability to predict conditions not used during identification remains to be demonstrated.

This reservation is particularly important for the interpretation of the sulfate parameters. Simultaneously seeking several parameters from a single time series can lead to different combinations of Deff, k, S and h producing similar curves. The fact that certain parameters are zero or of little influence in several formulations reduces, in practice, the effective dimension of the problem, but is not sufficient to demonstrate the uniqueness of the solutions. The absence of a formal sensitivity and identifiability analysis therefore constitutes an important methodological limitation. Multiple reinitializations of the L-BFGS-B algorithm, supplemented by local or global sensitivity analysis and, ideally, by the estimation of uncertainty intervals, would make it possible to verify the robustness of the identified parameters.

The exchange coefficient h, for its part, shows low dispersion between formulations, with values ranging between 8.0×10^{-8} and 1.2×10^{-7} m/s. This relative stability suggests that the differences observed between formulations are mainly related to the internal properties represented by Deff, k and S, rather than to a significant modification of the exchange conditions at the interface. This interpretation nonetheless remains cautious, as the apparent stability of h does not, on its own, constitute proof of this parameter's independent identifiability.

The differences observed between formulations must also be placed within the experimental framework used. The eight concretes have relatively close W/C ratios, ranging between 0.47 and 0.49, which limits the direct effect of this parameter, but the nature, particle size distribution and proportions of the aggregates differ. Formulations F1 and F3, made with crushed Brazzaville aggregates, thus exhibit the lowest porosity and Deff,NO3 values, while F5 and especially F6, made with rounded aggregates, exhibit higher porosities and higher diffusivities. This configuration makes it possible to study the influence of local materials within a relatively narrow range of W/C ratio, but it does not constitute a factorial experimental design allowing a variation in diffusivity to be independently attributed to each formulation parameter. The interpretation of the specific effect of aggregate nature must therefore remain associated with the simultaneous differences in particle size distribution, G/S ratio and real density.

The results thus show that accessible porosity constitutes a particularly relevant macroscopic descriptor of nitrate transport in the formulations studied, but that it cannot be considered a sufficient variable to explain all the observed behaviors. Differences between the more compact formulations may also depend on pore network connectivity, tortuosity, constrictivity and the characteristics of the interfacial transition zone, in accordance with microstructural approaches to transport in cementitious materials [44]. The absence of independent measurement of these parameters therefore constitutes an important limitation for a more advanced mechanistic interpretation.

The limitations of the numerical model must also be considered. The one-dimensional geometry adequately reproduces the diffusion setup used experimentally (§2.3.1), but it does not represent the lateral heterogeneities of real concrete, the explicit distribution of aggregates, local porosity gradients, or cracking effects. A two- or three-dimensional extension would be necessary to directly transpose the model to the scale of a structure, particularly when concentration gradients, material–environment interfaces and preferential transport pathways become significant [21].

Similarly, the identified parameters are assumed to be constant during the simulation, whereas transport properties evolve with hydration and the microstructural transformations of the cementitious matrix [45][46]. This assumption is particularly restrictive for sulfates, for which chemical reactions can progressively modify the composition and structure of the matrix. The first-order reaction kinetics adopted here constitute a deliberately parsimonious representation of the complex interactions between sulfates and cementitious phases, which may involve adsorption, dissolution, precipitation and modification of porosity [45]. The deviations observed at early diffusion times may in particular reflect the limitations of this simplified representation.

Another limitation concerns the representation of the boundary condition. The model does not explicitly reproduce the biweekly renewal of the external solution used in the experimental protocol (§2.1): the concentration in the sand zone may thus evolve during the simulation instead of remaining strictly fixed at the external concentration C_0. An explicit representation of solution renewal would bring the numerical condition closer to the experimental procedure and reduce a potential source of deviation between simulation and measurement.

For nitrates, the largest model deviations occur precisely for the most compact formulations, namely F1, F3 and F8. This trend indicates that the Fickian model used constitutes a satisfactory representation of overall behavior but does not fully reproduce the kinetics observed in these matrices. Accounting for additional phenomena, such as initial saturation conditions, delay effects, or a finer description of the pore structure, could improve this representation. This observation also constitutes an argument in favor of distinguishing between the overall quality of trend reproduction and the model's ability to reproduce all the temporal features of the experimental curves.

In this context, the originality of the study lies less in the isolated use of a diffusive model than in the combination of several levels of analysis: eight formulations using local Congolese aggregates, characterization of physical and mechanical properties, comparative transport of nitrates and sulfates, finite-volume modeling, and inverse identification of the transport parameters. This combination makes it possible to relate, within a single framework, the concrete formulation, its macroscopic properties, its transport behavior and, for sulfates, the possibility of an effective source term. The data available in the literature mainly concern different materials and exposure conditions; the value of the present work is therefore also to document the behavior of formulations using local aggregates in a humid tropical context that remains relatively underrepresented in studies on the coupled transport of nitrates and sulfates.

In terms of durability, these results finally show that prescriptive formulation or mechanical strength criteria alone are not necessarily sufficient to distinguish all ionic transfer performances. Within the domain studied, formulations F1 and F3 present the best compromise between low porosity, mechanical strength and low nitrate diffusivity. They should not, however, be considered automatically compliant with an XA2 or XA3 exposure class on the basis of these results alone. Similarly, the vulnerability of formulations F5 and F6 is here mainly associated with their diffusive behavior and porosity, whereas F7 stands out for sulfate behavior characterized by a marked effective release. These results thus reinforce the value of a performance-based approach in which the diffusion coefficient constitutes a complementary indicator to prescriptive durability criteria, in line with the general guidelines of the fib Model Code performance-based approaches [47] and with work devoted to the mechanistic assessment of the durability of cementitious materials [35].

By contrast, the results obtained over twelve weeks do not make it possible to directly extrapolate a long-term service life, nor to conclude that a given formulation would guarantee a service life exceeding several decades. Such an extrapolation would in particular require considering the temporal evolution of the transport parameters, mineralogical transformations, actual moisture conditions, cracking, and the simultaneous interactions between several aggressive species.

The priority perspectives thus concern first the formal verification of the identifiability and uncertainty of the sulfate parameters, followed by the introduction of a boundary condition explicitly reproducing the renewal of the external solution. They also concern the use of conservative fluxes at the interfaces between zones, the introduction of time- or microstructural-state-dependent transport parameters, the use of nonlinear reaction kinetics, and coupling with a geochemical model allowing the explicit representation of the evolution of cementitious phases. In the longer term, extension to multi-ionic transport simultaneously integrating nitrates, sulfates, chlorides and magnesium would make it possible to better represent the chemically complex environments to which hydraulic structures may be subjected.

Conclusion

This study has developed a numerical and experimental framework for analyzing the transport of nitrate and sulfate ions in eight concrete formulations made with local Congolese aggregates, combining finite-volume modeling of the sand–concrete–water–concrete–sand configuration, inverse parameter identification using L-BFGS-B, and microstructural analysis supported by SEM-EDS observations [10].

For nitrates, transport is described, as a first approximation, by a Fickian diffusion model. At 90 days, the effective diffusion coefficients range from 2.63×10^{-11} to 8.07×10^{-11} m²/s and exhibit a strong empirical relationship with accessible porosity ($R^2 = 0.986$). The model reproduces the relative ordering of the formulations but underestimates the concentrations of certain compact matrices (F1, F3, and F8), highlighting a limitation of a model based solely on effective diffusion.

For sulfates, the diffusion–reaction–source model identifies, a posteriori, three transport behaviors: diffusion-dominated transport for F6, diffusion–reaction transport for F5, and source-term-dominated behavior for F1–F4, F7, and F8. This latter regime is consistent, within the model framework, with an effective internal release of ions, with concentrations reaching up to 560 mg/L for F7. The identification of a diffusion coefficient alone is therefore insufficient to characterize sulfate transport.

Cross-analysis shows that accessible porosity is a major factor governing diffusivity, while aggregate type and particle-size distribution also contribute to the behavior of the formulations. F1 and F3 combine low porosity, high compressive strength, and low nitrate diffusivity. Conversely, F5 and F6 exhibit higher diffusivity associated with higher porosity, whereas F7 exhibits a distinct sulfate transport behavior characterized by a relatively high source term.

These results show that the water-to-cement ratio and mechanical strength alone are insufficient to characterize the durability of concrete in aggressive environments. Accessible porosity, the effective diffusion coefficient and, for sulfates, the reaction and release parameters constitute relevant complementary indicators. The characteristics observed for F1 and F3 indicate potentially favorable transport properties for structures exposed to aggressive environments; however, the present results do not demonstrate compliance with the XA2–XA3 exposure classes of EN 206.

Finally, the results highlight the value of a performance-based approach founded on effective transport properties. The main perspectives include assessing the identifiability of the sulfate-model parameters, validating the model against independent and longer-term datasets, introducing nonlinear kinetics and evolving transport properties, extending the model to other aggressive species, and coupling the transport model with microstructural and probabilistic durability approaches.

Declarations

Funding Declaration

This research received no external funding.

Clinical Trial Registration

NOT APPLICABLE.

Corresponding Author

nar6malanda@gmail.com

Consent to Publish declaration

Not applicable.

Ethics and Consent to Participate declarations

Not applicable.

References

[1] Ebata-Ndion B, Makela JB, Mangala SCM, Malanda N (2026) Experimental Study of the Diffusion of Nitrate and Sulfate Ions through Concrete in the Case of Underground Water Reservoirs and the Impact on Their Durability. *Geomaterials* **16**:127–158. https://doi.org/10.4236/gm.2026.163008

[2] Crank J (1975) The Mathematics of Diffusion, 2nd edn. Oxford University Press, Oxford.

[3] Taylor HFW (1997) Cement Chemistry, 2nd edn. Thomas Telford Publishing, London. https://doi.org/10.1680/cc.25929

[4] Skalny J, Marchand J, Odler I (2002) Sulfate Attack on Concrete. Spon Press, London.

[5] Marchand J, Samson E, Maltais Y, Beaudoin JJ (2002) Theoretical Analysis of the Effect of Weak Sodium Sulfate Solutions on the Durability of Concrete. *Cement and Concrete Composites* **24**:317–329. https://doi.org/10.1016/S0958-9465(01)00083-X

[6] Lothenbach B, Le Saout G, Gallucci E, Scrivener K (2008) Influence of Limestone on the Hydration of Portland Cements. *Cement and Concrete Research* **38**:848–860. https://doi.org/10.1016/j.cemconres.2008.01.002

[7] Marko M, Hrubý P, Janča M, Kříkala J, Hajzler J, Šoukal F, Vojtíšek J, Doležal M (2022) Monitoring of Ion Mobility in the Cement Matrix to Establish Sensitivity to the ASR Caused by External Sources. *Materials* **15**:4730. https://doi.org/10.3390/ma15144730

[8] Taylor HFW, Famy C, Scrivener KL (2001) Delayed Ettringite Formation. *Cement and Concrete Research* **31**:683–693. https://doi.org/10.1016/S0008-8846(01)00466-5

[9] Makela JB, Ebata-Ndion B, Malanda N, Mbeke SK (2025) Prospective Study and Physico-Mechanical Characterisation of Granular Materials Used in the Manufacture of Ordinary Concrete in Congo. *Geomaterials* **15**:1–24. https://doi.org/10.4236/gm.2025.151001

[10] Makela JB, Ceti CAM, Sodjinou RD, Mfoutou NN, Malanda N (2026) Microstructural Study of Common Concrete Manufactured in Congo-Brazzaville. *Open Journal of Civil Engineering* **16**:37–59. https://doi.org/10.4236/ojce.2026.161003

[11] NF EN 12390-2: Essais pour béton durci — Partie 2 : Confection et conservation des éprouvettes pour essais de résistance. Saint-Denis La Plaine, AFNOR. https://www.boutique.afnor.org/fr-fr/norme/nf-en-123902/essais-pour-beton-durci-partie-2-confection-et-conservation-des-eprouvettes/fa155373/39064

[12] Malanda N, Ndion BE, Tathy C, Mongo T, Louzolokimbembe P (2024) Identification of the Diffusion Coefficients of Pollutants (NO_3^- and Mn^{2+}) through the Walls of Concrete Tank and Vulnerability of the Stored Water Quality. *Engineering* **16**:246–274. https://doi.org/10.4236/eng.2024.169019

[13] Bear J (1972) Dynamics of Fluids in Porous Media. Elsevier, New York.

[14] Knabner P, Angermann L (2003) Numerical Methods for Elliptic and Parabolic Partial Differential Equations. Springer, New York. https://doi.org/10.1007/b97419

[15] Patankar SV (1980) Numerical Heat Transfer and Fluid Flow. Hemisphere Publishing Corporation, New York.

[16] Lasaga AC (1998) Kinetic Theory in the Earth Sciences. Princeton University Press, Princeton.

[17] Atkins P, de Paula J (2010) Physical Chemistry, 9th edn. Oxford University Press, Oxford.

[18] Samson E, Marchand J, Snyder KA (2003) Calculation of Ionic Diffusion Coefficients on the Basis of Migration Test Results. *Materials and Structures* **36**:156–165. https://doi.org/10.1007/BF02479554

[19] Neville AM (2011) Properties of Concrete, 5th edn. Pearson Education, Harlow.

[20] Mehta PK, Monteiro PJM (2014) Concrete: Microstructure, Properties, and Materials, 4th edn. McGraw-Hill Education, New York.

[21] Bentz DP, Garboczi EJ (1991) Percolation of Phases in a Three-Dimensional Cement Paste Microstructural Model. *Cement and Concrete Research* **21**:325–344. https://doi.org/10.1016/0008-8846(91)90014-9

[22] Garboczi EJ (1990) Permeability, Diffusivity, and Microstructural Parameters: A Critical Review. *Cement and Concrete Research* **20**:591–601. https://doi.org/10.1016/0008-8846(90)90101-3

[23] Powers TC (1958) Structure and Physical Properties of Hardened Portland Cement Paste. *Journal of the American Ceramic Society* **41**:1–6. https://doi.org/10.1111/j.1151-2916.1958.tb13494.x

[24] Winslow DN, Cohen MD, Bentz DP, Snyder KA, Garboczi EJ (1994) Percolation and Pore Structure in Mortars and Concrete. *Cement and Concrete Research* **24**:25–37. https://doi.org/10.1016/0008-8846(94)90079-5

[25] Samson E, Marchand J (2007) Modeling the Transport of Ions in Unsaturated Cement-Based Materials. *Computers & Structures* **85**:1740–1756. https://doi.org/10.1016/j.compstruc.2007.04.008

[26] Scrivener KL, Crumbie AK, Laugesen P (2004) The Interfacial Transition Zone (ITZ) between Cement Paste and Aggregate in Concrete. *Interface Science* **12**:411–421. https://doi.org/10.1023/b:ints.0000042339.92990.4c

[27] Bird RB, Stewart WE, Lightfoot EN (2002) Transport Phenomena, 2nd edn. John Wiley & Sons, New York.

[28] Tian B, Cohen MD (2000) Does Gypsum Formation during Sulfate Attack on Concrete Lead to Expansion? *Cement and Concrete Research* **30**:117–123. https://doi.org/10.1016/S0008-8846(99)00211-2

[29] Carde C, François R (1999) Modelling the Loss of Strength and Porosity Increase Due to the Leaching of Cement Pastes. *Cement and Concrete Composites* **21**:181–188. https://doi.org/10.1016/S0958-9465(98)00046-8

[30] Steefel CI, DePaolo DJ, Lichtner PC (2005) Reactive Transport Modeling: An Essential Tool and a New Research Approach for the Earth Sciences. *Earth and Planetary Science Letters* **240**:539–558. https://doi.org/10.1016/j.epsl.2005.09.017

[31] Santhanam M, Cohen MD, Olek J (2003) Effects of Gypsum Formation on the Performance of Cement Mortars during External Sulfate Attack. *Cement and Concrete Research* **33**:325–332. https://doi.org/10.1016/S0008-8846(02)00955-9

[32] Glasser FP, Marchand J, Samson E (2008) Durability of Concrete—Degradation Phenomena Involving Detrimental Chemical Reactions. *Cement and Concrete Research* **38**:226–246. https://doi.org/10.1016/j.cemconres.2007.09.015

[33] Müllauer W, Beddoe RE, Heinz D (2013) Sulfate Attack Expansion Mechanisms. *Cement and Concrete Research* **52**:208–215. https://doi.org/10.1016/j.cemconres.2013.07.005

[34] CEN (2013) EN 206:2013+A1:2016 — Concrete: Specification, Performance, Production and Conformity. European Committee for Standardization, Brussels.

[35] Beushausen H, Torrent R, Alexander MG (2019) Performance-Based Approaches for Concrete Durability: State of the Art and Future Research Needs. *Cement and Concrete Research* **119**:11–20. https://doi.org/10.1016/j.cemconres.2019.01.003

[36] Hooton RD (2019) Future Directions for Design, Specification, Testing, and Construction of Durable Concrete Structures. *Cement and Concrete Research* **124**:105827. https://doi.org/10.1016/j.cemconres.2019.105827

[37] Shafikhani M, Chidiac SE (2019) Quantification of Concrete Chloride Diffusion Coefficient — A Critical Review. *Cement and Concrete Composites* **99**:225–250. https://doi.org/10.1016/j.cemconcomp.2019.03.011

[38] Alexander M, Bertron A, De Belie N (2012) Performance of Cement-Based Materials in Aggressive Aqueous Environments. Springer, Dordrecht.

[39] Baroghel-Bouny V (2007) Water Vapour Sorption Experiments on Hardened Cementitious Materials. Part I — Essential Tool for Analysis of Hygral Behaviour and Its Relation to Pore Structure. *Cement and Concrete Research* **37**:414–437. https://doi.org/10.1016/j.cemconres.2006.11.019

[40] fib – Fédération internationale du béton (2013) fib Model Code for Concrete Structures 2010. Ernst & Sohn / Wiley, Berlin. https://doi.org/10.1002/9783433604090

[41] Xie L, Liu L, Tao G (2023) Study on the Quantitative Relationship between Diffusivity and Pore Structure Parameters of Cement Pastes. *Magazine of Concrete Research* **75**:1040–1050. https://doi.org/10.1680/jmacr.22.00262

[42] Tang L, Nilsson L-O (1992) Rapid Determination of the Chloride Diffusivity in Concrete by Applying an Electric Field. *ACI Materials Journal* **89(1)**:49–53. https://doi.org/10.14359/1244

[43] Atkinson A (1985) The Time Dependence of pH within a Repository for Radioactive Waste Disposal. UK Atomic Energy Authority Report, Harwell.

[44] Zhang Y, Ye G, Yang Z (2020) Pore Size Dependent Connectivity and Ionic Transport in Saturated Cementitious Materials. *Construction and Building Materials* **238**:117680. https://doi.org/10.1016/j.conbuildmat.2019.117680

[45] Patel RA, Perko J, Jacques D, De Schutter G, Ye G, Van Breugel K (2018) Effective Diffusivity of Cement Pastes from Virtual Microstructures: Role of Gel Porosity and Capillary Pore Percolation. *Construction and Building Materials* **165**:833–845. https://doi.org/10.1016/j.conbuildmat.2018.01.010

[46] De Weerdt K, Haha MB, Le Saout G, Kjellsen KO, Justnes H, Lothenbach B (2011) Hydration Mechanisms of Ternary Portland Cements Containing Limestone Powder and Fly Ash. *Cement and Concrete Research* **41**:279–291. https://doi.org/10.1016/j.cemconres.2010.11.014

[47] Hooton RD, Bickley JA (2012) Prescriptive versus Performance Approaches for Durability Design—The End of Innocence? *Materials and Corrosion* **63**:1097–1101. https://doi.org/10.1002/maco.201206780